

Thermodynamic geometry of friction on graphs: Resistance, commute times, and optimal transport

Jordan R. Sawchuk* and David A. Sivak†

Department of Physics, Simon Fraser University, Burnaby, British Columbia, Canada V5A 1S6

(Dated: January 6, 2026)

We demonstrate that for slowly driven reversible Markov chains, the thermodynamic friction metric governing dissipation is equivalent to two independently developed graph-theoretic geometries: commute-time geometry and resistance distance. This equivalence yields complementary physical insights: the commute-time metric provides the local Euclidean description of the thermodynamic manifold, while the resistance distance maps dissipation to power loss in an electrical network. We further show that this metric arises from a discrete L^2 -Wasserstein transport cost evaluated along paths of equilibrium distributions, extending a correspondence previously shown for continuous-state processes. These results unify linear-response, electrical-resistance, random-walk, and optimal-transport frameworks, revealing linear-response dissipation as the energetic cost of transporting probability through the intrinsic geometry of the state-space network.

I. INTRODUCTION

Geometric ideas have long played a role in thermodynamics, from Riemannian formulations of equilibrium states to geometric treatments of fluctuations and information [1–4]. For driven stochastic systems, a robust metric structure emerges in the linear-response (LR) regime: the mean excess power dissipated under slow driving equals the squared velocity of the control parameters with respect to a *friction metric* defined by time-integrated force-force correlations [5]. Control protocols that minimize the excess work are geodesics on this thermodynamic manifold. Recently, this thermodynamic framework was connected to optimal-transport (OT) theory [6], revealing that for continuous overdamped dynamics, the thermodynamic distance coincides with the L^2 -Wasserstein distance restricted to paths of equilibrium distributions.

Independently, geometries of weighted graphs have emerged in network science [7–12]. In *commute-time geometry*, the states of a Markov chain are embedded in Euclidean space such that squared distances between states equals the mean round-trip random-walk time [13]. Closely related is the *resistance distance*, defined as the effective electrical resistance between nodes in a resistor network constructed on the Markov graph [14, 15]. Despite their common dynamical origins, these graph-theoretic geometries have not previously been connected to the thermodynamic geometry of driven processes.

We demonstrate that for discrete reversible continuous-time Markov chains, these three geometric frameworks are physically equivalent representations of the same underlying metric structure. This equivalence maps LR dissipation to Joule heating in a resistor network where node potentials are deviations from equilibrium and edge currents are probability fluxes.

We exploit this isomorphism to derive exact analytical friction metrics for linear and cyclic graphs. Complementarily, the commute-time embedding provides a local Euclidean description of the thermodynamic manifold, revealing entropic and energetic bottlenecks as distances that are costly to traverse. Further, we extend the restricted control-transport correspondence to graphs via a discrete Benamou-Brenier cost along paths of equilibrium distributions.

II. THEORETICAL BACKGROUND

We consider a driven, ergodic, continuous-time Markov chain on a finite state space Ω with $|\Omega| = n+1$. The probability distribution $\mathbf{p}_s = (p_s(x))_{x \in \Omega}$ evolves according to the master equation

$$\frac{1}{\tau_{\text{prot}}} \partial_s \mathbf{p}_s = \mathbb{W}_s \mathbf{p}_s , \quad (1)$$

where $s \in [0, 1]$ is the time rescaled by the total protocol duration τ_{prot} . Control is assumed to be *conservative*: the time-dependence of the transition-rate matrix $\mathbb{W}_s \equiv \mathbb{W}(\mathbf{V}_s)$ is driven by changing state energies $\mathbf{V}_s \in \mathbb{R}^{n+1}$. At fixed s , the dynamics are reversible, so that the transition rates $w_s(x|y)$ (the off-diagonal elements of \mathbb{W}_s) satisfy detailed balance $w_s(x|y)\pi_s(y) = w_s(y|x)\pi_s(x)$, for instantaneous equilibrium distribution $\pi_s(x) \propto e^{-\beta V_s(x)}$.

Assuming that the system begins in equilibrium at $s = 0$, in the quasistatic limit ($\tau_{\text{prot}} \rightarrow \infty$) $\mathbf{p}_s = \boldsymbol{\pi}_s$ for all s , and the mean dissipated work $\langle \mathcal{W} \rangle$ equals the net change in free energy, ΔF . For finite-but-slow driving, the small lag $\delta \mathbf{p}_s \equiv \mathbf{p}_s - \boldsymbol{\pi}_s$ between the actual distribution and the equilibrium distribution produces a mean *excess* work $\langle \mathcal{W}_{\text{ex}} \rangle \equiv \langle \mathcal{W} \rangle - \Delta F = \tau_{\text{prot}}^{-1} \int_0^1 ds \delta \mathbf{p}_s^\top \dot{\mathbf{V}}_s$ given in the linear-response approximation by

$$\langle \mathcal{W}_{\text{ex}} \rangle^{(\text{LR})} = \frac{1}{\tau_{\text{prot}}} \int_0^1 ds \dot{\mathbf{V}}_s^\top \zeta_{\mathbf{V}_s} \dot{\mathbf{V}}_s , \quad (2)$$

* jordan_sawchuk@sfu.ca

† dsivak@sfu.ca

where the *friction tensor* $\zeta_V = -\beta \mathbb{W}^D \text{diag}\{\boldsymbol{\pi}\}$ captures the system's time-integrated relaxation [5, 16]. Here \mathbb{W}_s^D is the Drazin inverse of the rate matrix [16]. The friction tensor acts as a metric on the manifold of discrete energy “landscapes” \mathbf{V} , and the excess power is the squared velocity $\|\mathbf{V}_s\|_\zeta^2$ measured in this metric. Through most of this paper, we omit explicit dependence on s .

For reversible dynamics, the mapping $\mathbf{V} \leftrightarrow \boldsymbol{\pi}$ is bijective up to a global energy shift. Therefore, the same geometry can be expressed on the space of probability distributions, the (open) *probability simplex*

$$\Delta^n = \{\mathbf{p} \in \mathbb{R}^{n+1} : \mathbf{1}^\top \mathbf{p} = 1, p(x) > 0\} . \quad (3)$$

The metric g_π on Δ^n is obtained by requiring invariance of excess power under this change of coordinates: $(d\boldsymbol{\pi})^\top g_\pi (d\boldsymbol{\pi}) = (d\mathbf{V})^\top \zeta_V (d\mathbf{V})$. One finds that

$$\beta g_\pi = -\text{diag}\{\boldsymbol{\pi}\}^{-1} \mathbb{W}^D . \quad (4)$$

The simplex Δ^n for an $(n+1)$ -state system is an n -dimensional manifold whose tangent space $T_\pi \Delta^n$ is the set of all vectors orthogonal to the ones vector $\mathbf{1}$. An $(n+1) \times (n+1)$ representation of a metric on Δ^n is thus non-unique. We will say that two representations g and g' are *equivalent* on Δ^n if they define the same length element on the tangent space, written

$$g \stackrel{\Delta^n}{\sim} g' \iff \dot{\boldsymbol{\pi}}^\top g \dot{\boldsymbol{\pi}} = \dot{\boldsymbol{\pi}}^\top g' \dot{\boldsymbol{\pi}}, \quad \forall \dot{\boldsymbol{\pi}} \in T_\pi \Delta^n . \quad (5)$$

Most applications consider parametric control, i.e., the equilibrium distribution depends smoothly on a low-dimensional set of control parameters \mathbf{u} so that $\boldsymbol{\pi}_s = \boldsymbol{\pi}(\mathbf{u}_s)$. The metric (4) on the probability simplex then induces a metric on the control-parameter submanifold $\tilde{\zeta}_{ij}(\mathbf{u}) = \sum_{x,y} g_{\boldsymbol{\pi}(\mathbf{u})}(x,y) \partial_i \pi(x) \partial_j \pi(y)$ [16] (note that we use subscripts to index partial-control parameters and arguments to index states). Thus all results that follow apply equally to parametric control, with the same equivalence class of metrics governing dissipation.

III. EQUIVALENCE OF LINEAR-RESPONSE, COMMUTE-TIME, AND RESISTANCE GEOMETRIES

To establish the equivalence of linear-response and graph-theoretic geometries, we associate the Markov chain with a graph $G = (\Omega, \mathcal{E})$ with vertex set Ω and edges $(x, y) \in \mathcal{E}$ connecting states with nonzero transition rates. By detailed balance, we may assign symmetric edge *conductances*

$$c(x, y) \equiv w(x|y)\pi(y) = w(y|x)\pi(x) , \quad (6)$$

interpreted as the directed equilibrium probability flux. The weighted graph Laplacian is the symmetric matrix

$$L(x, y) = \begin{cases} -c(x, y) & x \neq y \\ \sum_{z \neq x} c(x, z) & x = y \end{cases} , \quad (7)$$

or $L = -\mathbb{W} \text{diag}\{\boldsymbol{\pi}\}$. The friction metric (4) and the Moore-Penrose pseudoinverse L^+ [17] of L have the same spectrum but differ in their nullspaces: The nullspace of βg is spanned by $\boldsymbol{\pi}$, and the nullspace of L^+ is spanned by $\mathbf{1}$. That is,

$$\beta g = (I - \boldsymbol{\pi} \mathbf{1}^\top)^\top L^+ (I - \boldsymbol{\pi} \mathbf{1}^\top) , \quad (8)$$

for projector $I - \boldsymbol{\pi} \mathbf{1}^\top$. This projector acts as the identity on all admissible $\dot{\boldsymbol{\pi}}$, and thus

$$\beta g \stackrel{\Delta^n}{\sim} L^+ . \quad (9)$$

In circuit theory, the effective resistance between nodes x, y for a circuit with edge resistances $r(x, y) = [c(x, y)]^{-1}$ is determined by the same pseudoinverse [15, 18]:

$$R_{\text{eff}}(x, y) = (\hat{\mathbf{e}}_x - \hat{\mathbf{e}}_y)^\top L^+ (\hat{\mathbf{e}}_x - \hat{\mathbf{e}}_y) , \quad (10)$$

for standard basis vectors $\hat{\mathbf{e}}_x, \hat{\mathbf{e}}_y$. Expanding this in the elements of L^+ , it follows immediately from the definition of the tangent space that $R_{\text{eff}} \stackrel{\Delta^n}{\sim} -2L^+$, and thus

$$\beta g \stackrel{\Delta^n}{\sim} -\frac{1}{2} R_{\text{eff}} . \quad (11)$$

Finally, the mean commute time $C(x, y)$ between states x and y is defined as the average time to travel from y to x and back again (or vice versa),

$$C(x, y) \equiv \tau_{\text{mfp}}(x|y) + \tau_{\text{mfp}}(y|x) , \quad (12)$$

for mean first-passage times (MFPTs) $\tau_{\text{mfp}}(x|y) \equiv \langle \inf \{t : X_t = x\} \mid X_0 = y \rangle$. Using the relation

$$\mathbb{W}^D = -\text{diag}\{\boldsymbol{\pi}\} \mathcal{T}_{\text{mfp}} (I - \boldsymbol{\pi} \mathbf{1}^\top) \quad (13)$$

between the Drazin inverse of the rate matrix and the MFPTs [19] [here \mathcal{T}_{mfp} is the matrix whose x, y component is $\tau_{\text{mfp}}(x|y)$], direct substitution into Eq. (4) yields $\beta g = -\mathcal{T}_{\text{mfp}}(I - \boldsymbol{\pi} \mathbf{1}^\top)$. Omitting the projector $I - \boldsymbol{\pi} \mathbf{1}^\top$ as before and symmetrizing \mathcal{T}_{mfp} (permissible since the asymmetric part of a matrix does not contribute to a quadratic form), we have our final metric equivalence

$$\beta g \stackrel{\Delta^n}{\sim} -\frac{1}{2} C \quad (14)$$

with $C \equiv \mathcal{T}_{\text{mfp}} + \mathcal{T}_{\text{mfp}}^\top$.

The metric equivalences (9), (11), and (14) constitute the central result of this paper. These show that the LR thermodynamic, resistance, and commute-time ge-

ometries are different manifestations of the same graph structure. The implications are explored further in Sections V and VI.

IV. THERMODYNAMIC DISTANCE AND OPTIMAL TRANSPORT ON GRAPHS

We now show that the squared thermodynamic distance

$$\mathcal{L}^2(\boldsymbol{\pi}_0, \boldsymbol{\pi}_1) \equiv \inf_{\dot{\boldsymbol{\pi}}_s} \int_0^1 ds \dot{\boldsymbol{\pi}}_s^\top (\beta g) \dot{\boldsymbol{\pi}}_s \quad (15)$$

between equilibrium distributions $\boldsymbol{\pi}_0, \boldsymbol{\pi}_1 \in \Delta^n$ equals a discrete L^2 -Wasserstein transport cost evaluated along paths of equilibrium distributions, extending a previous result for overdamped Langevin dynamics [6].

First, recall the Benamou-Brenier formulation of the L^2 -Wasserstein distance: the L^2 -Wasserstein distance between two absolutely continuous densities ρ_0, ρ_1 on \mathbb{R}^d is [20, 21]

$$\mathcal{W}_2^2(\rho_0, \rho_1) = \inf_{\dot{\rho}_s = -\nabla \cdot (\rho_s \nabla \phi_s)} \int_0^1 ds \int dx \rho_s(x) |\nabla \phi_s(x)|^2. \quad (16)$$

To construct an analog of (16) for reversible Markov dynamics on a graph, the machinery of discrete calculus [22] is required to replace continuum vector fields and differential operators with their discrete counterparts. For Markov graph $G = (\Omega, \mathcal{E})$, functions on vertices (“scalar fields”) and functions on edges (“vector fields”) live in different Hilbert spaces, respectively $\mathcal{H}(\Omega)$ and $\mathcal{H}(\mathcal{E})$. The *graph gradient* $\nabla_G : \mathcal{H}(\Omega) \rightarrow \mathcal{H}(\mathcal{E})$ and *graph divergence* $\text{div}_G : \mathcal{H}(\mathcal{E}) \rightarrow \mathcal{H}(\Omega)$ map functions between these spaces. The inner products $(\cdot, \cdot)_{\mathcal{H}(\Omega)}$ and $(\cdot, \cdot)_{\mathcal{H}(\mathcal{E})}$ are required to obey an adjointness relation analogous to integration by parts,

$$(\nabla_G \varphi, \Psi)_{\mathcal{H}(\mathcal{E})} = (\varphi, -\text{div}_G \Psi)_{\mathcal{H}(\Omega)}, \quad (17)$$

and must reproduce the graph Laplacian (7) in the sense that

$$\psi^\top L \psi = (\psi, -\text{div}_G \nabla_G \psi)_{\mathcal{H}(\Omega)}. \quad (18)$$

The choice of inner products and differential operators is not unique. Here we follow the conventions of [23], defining the weighted inner products

$$(\psi, \varphi)_{\mathcal{H}(\Omega)} = \sum_{x \in \Omega} \pi(x) \psi(x) \varphi(x) \quad (19a)$$

$$(\Psi, \Phi)_{\mathcal{H}(\mathcal{E})} = \frac{1}{2} \sum_{x, y \in \Omega} w(x|y) \pi(y) \Psi(x, y) \Phi(x, y) \quad (19b)$$

and gradient and divergence operators

$$(\nabla_G \psi)(x, y) \equiv \psi(y) - \psi(x) \quad (20a)$$

$$(\text{div}_G \Psi)(x) \equiv \frac{1}{2} \sum_{y \in \Omega} w(y|x) [\Psi(y, x) - \Psi(x, y)]. \quad (20b)$$

For any smooth path $[0, 1] \ni s \mapsto \boldsymbol{\pi}_s \in \Delta^n$, define a velocity potential ϕ_s (unique up to an additive constant) by

$$\dot{\boldsymbol{\pi}}_s = L_s \phi_s. \quad (21)$$

Thus $\phi_s^\top L_s \phi_s = \dot{\boldsymbol{\pi}}_s^\top (\beta g) \dot{\boldsymbol{\pi}}_s$, so via (17) and (18) the squared thermodynamic distance between two equilibrium distributions $\boldsymbol{\pi}_0, \boldsymbol{\pi}_1$ is

$$\mathcal{L}^2(\boldsymbol{\pi}_0, \boldsymbol{\pi}_1) = \inf_{\dot{\boldsymbol{\pi}}_s = L_s \phi_s} \int_0^1 ds \|\nabla_G \phi_s\|_{\mathcal{H}(\mathcal{E})}^2. \quad (22)$$

The potential differences $(\nabla_G \phi_s)(x, y) = \phi_s(y) - \phi_s(x)$ generate probability currents across the edges of the graph, and $\|\nabla_G \phi_s\|_{\mathcal{H}(\mathcal{E})}^2$ measures the instantaneous dissipative cost of those currents. We clarify the probabilistic interpretation of these potentials and currents in Sec. V C.

Equation (22) is a discrete analog of the Benamou-Brenier formula (16), with the equilibrium weights absorbed into the inner product (19b). The constraint $\dot{\boldsymbol{\pi}}_s = L_s \phi_s$ acts as a continuity equation, analogous to the mass-conservation law $\dot{\rho}_s = -\nabla \cdot (\rho_s \nabla \phi_s)$ for continuous spaces. Though there is a formal difference between these expressions (the density appears in a flux of the form $\pi_s \nabla \phi_s$ in the continuous case, whereas it is incorporated into the operator L in the discrete setting), both structures encode the same geometric relation between a potential field and the induced probability flow. Thus the LR thermodynamic geometry on Δ^n coincides with a discrete L^2 -Wasserstein geometry defined by the graph Laplacian. In App. A, we identify this result as a special case of the discrete L^2 -Wasserstein metric introduced in [23, 24].

V. GEOMETRIC AND PHYSICAL INTERPRETATIONS

A. Commute-time embedding and bottlenecks

In Sec. III we showed that the friction metric g and the commute-time matrix C encode the same geometry on the probability simplex Δ^n . A classical result states that C is a *squared Euclidean distance matrix* [13]: there exists a mapping $\Omega \ni x \mapsto \mathbf{a}(x) \in \mathbb{R}^m$ with $m \leq n = |\Omega| - 1$ such that

$$C(x, y) = \|\mathbf{a}(x) - \mathbf{a}(y)\|^2. \quad (23)$$

Through this embedding the Markov graph—a purely topological construction—acquires a geometry in which each state x sits at a point $\mathbf{a}(x) \in \mathbb{R}^m$.

A simple example illustrates the physical significance of this embedding: consider a small shift of probability from y to x : $d\pi = \epsilon(\hat{\mathbf{e}}_x - \hat{\mathbf{e}}_y)$, $0 < \epsilon \ll 1$. Then the increment of work is

$$\langle d\mathcal{W}_{\text{ex}} \rangle^{(\text{LR})} = \epsilon^2 k_B T \|\mathbf{a}(x) - \mathbf{a}(y)\|^2. \quad (24)$$

That is, the linear-response cost of transferring probability between two states is proportional to the squared distance between them in the commute-time embedding. For general $d\pi$, the work increment is

$$\langle d\mathcal{W}_{\text{ex}} \rangle^{(\text{LR})} = k_B T \|A^T d\pi\|^2, \quad (25)$$

where $A(x, \cdot) = \mathbf{a}(x)$. The matrix A may be obtained from C via classical multidimensional scaling [25]. Equation (25) admits a centroid interpretation: states with positive (negative) increments define a weighted centroid of probability-increasing (probability-decreasing) states in the Euclidean embedding, and the cost of transport is the squared distance between these centroids.

Geometrically, the commute-time embedding characterizes the locally Euclidean structure of the thermodynamic manifold, in the sense that the line element $d\ell \equiv [d\pi^T(\beta g)d\pi]^{1/2}$ is locally Cartesian in the coordinates $dx_i = (A^T d\pi)(x_i)$:

$$d\ell = \sqrt{(dx_0)^2 + (dx_1)^2 + \cdots + (dx_n)^2}. \quad (26)$$

The commute-time embedding also reveals bottlenecks in the dynamics. States that are close in the embedding form *clusters*—sets of states with relatively short pairwise commute times. Large gaps between clusters are bottlenecks. Equation (25) says that transport of probability mass between clusters is expensive, while redistributing mass within a cluster is cheap.

We mark two distinct origins for such bottlenecks, which we refer to as *entropic* and *energetic* bottlenecks by analogy to existing notions [26, 27]. Entropic bottlenecks arise when few transition pathways connect two clusters of states: Even when inter-cluster rates are comparable to intra-cluster rates, a sparse connectivity forces trajectories through narrow channels. Such bottlenecks are topological and cannot be removed by conservative control, so there is an unavoidable cost of moving probability between clusters separated by an entropic bottleneck. Energetic bottlenecks occur when the allowed paths between two regions involve at least one intermediate state with a large energy, creating long relaxation times and thus large commute distances between the regions. These energetic bottlenecks can occur even when there are many available transition paths, and as they originate in the potential landscape, they can often be mitigated by control parameters that lower relative barrier heights.

B. Linear-response dissipation as Joule heating

The equivalence $\beta g \stackrel{\Delta^n}{\sim} -\frac{1}{2}R_{\text{eff}}$ established in Sec. III gives a complementary physical picture: to each edge $(x, y) \in \mathcal{E}$ is associated a resistor with resistance $r(x, y) = [w(x|y)\pi(y)]^{-1}$. The discrete continuity equation $\dot{\pi} = L\phi$ introduced in Sec. IV may then be written as

$$\dot{\pi}(x) = \sum_y i(x, y), \quad (27)$$

for edge currents (directed from y to x)

$$i(x, y) = \frac{\phi(x) - \phi(y)}{r(x, y)}. \quad (28)$$

Equation (28) is Ohm's law for node potentials $-\phi(x)$ and edge currents $i(x, y)$. The linear-response excess work is then

$$\langle \mathcal{W}_{\text{ex}} \rangle^{(\text{LR})} = \frac{k_B T}{2\tau} \int_0^1 ds \sum_{x,y} r_s(x, y) i_s(x, y)^2. \quad (29)$$

The integrand is precisely the power dissipated in a resistor circuit: driving probability currents $i_s(x, y)$ incurs a quadratic cost governed by the instantaneous edge resistances $r_s(x, y)$.

C. Node potentials and edge currents

The scalar field ϕ now appears (up to sign convention) as both the electrical potential generating edge currents in the resistor network and the velocity potential generating probability fluxes in the discrete OT formulation. We now provide a more direct probabilistic interpretation of $\phi(x)$, and in doing so, we clarify the nature of the edge currents $i(x, y)$.

The linear-response approximation of the lag δp implicit in the friction-tensor formalism is [16, 28, 29]

$$\delta p \approx \delta p^{(\text{LR})} \equiv \tau^{-1} \tau_{\text{prot}} \mathbb{W}^{\mathcal{D}} \dot{\pi}. \quad (30)$$

Taking (without loss of generality) the gauge $\langle \phi \rangle_{\pi} = 0$, combining Eqs. (21) and (30) yields

$$-\phi(x) = \frac{\tau_{\text{prot}} \delta p^{(\text{LR})}(x)}{\pi(x)}. \quad (31)$$

The electric potential $-\phi(x)$ thus coincides with the excess probability at x relative to the equilibrium distribution. Substituting this into (28) and applying detailed balance gives

$$\frac{i(x, y)}{\tau_{\text{prot}}} = w(x|y) p^{(\text{LR})}(y) - w(y|x) p^{(\text{LR})}(x). \quad (32)$$

The edge currents $i(x, y)$ are thus precisely the (unit-

less) probability currents in the linear-response approximation, due to relaxation of the small deviation from equilibrium captured in the node potentials $\phi(x)$. Note that since the lag $\delta p^{(\text{LR})}(x)$ is assumed to be $\mathcal{O}(\tau_{\text{prot}}^{-1})$, the currents and node potentials are $\mathcal{O}(1)$ in τ_{prot} .

VI. METRICS FOR ELEMENTARY TOPOLOGIES

The electrical analogy established in Sec. V B allows the use of standard circuit-theoretical techniques like series/parallel reduction and Kron reduction [30] to simplify calculation of the friction metric. For simple topologies, we may instead derive closed-form expressions for the currents. In this section, we derive exact results for driven linear and cyclic graphs.

A. Linear graph

Consider a chain of $n + 1$ states connected by n edges $(x, x + 1)$. We label edges by the lower node value as in Fig. 1a, and we denote edge currents by $i_0(x)$ (adding the subscript 0 in anticipation of their role as a reference current for the cyclic graph). Because there are no loops, the continuity equation (27) can be inverted as

$$i_0(x) = \sum_{y=0}^x \dot{\pi}(y) \equiv \dot{\Pi}(x) , \quad (33)$$

for equilibrium cumulative distribution function $\Pi(x)$. For an arbitrary set of m control parameters $\mathbf{u} = \{u^0, u^1, \dots, u^{m-1}\}$ we have (with Einstein summation over parameter indices) $\dot{\Pi}(x) = \partial_i \Pi(x) u^i$, so

$$\langle \mathcal{P}_{\text{ex}} \rangle^{(\text{LR})} = \sum_{x=0}^{n-1} \underbrace{\frac{\partial_i \Pi(x) \partial_j \Pi(x)}{k_B T c(x)}}_{= \tilde{\zeta}_{ij}} \dot{u}^i \dot{u}^j , \quad (34)$$

from which we immediately identify the partial-control friction metric $\tilde{\zeta}_{ij}$. This is the discrete analog of the friction tensor $\tilde{\zeta}_{ij} = \int dx \frac{\partial_i \Pi(x) \partial_j \Pi(x)}{D\pi(x)}$ for 1D overdamped Langevin dynamics [31], with $\sum \rightarrow \int dx$ and $c(x) \rightarrow \beta D\pi(x)$. This limit for the conductance is in agreement with recent work showing that the symmetrized flux across an edge (identical to $c(x)$ under detailed balance) becomes $\beta D\pi(x)$ in the continuous limit [32].

B. Cycle graph

A cycle graph (Fig. 1b) is formed by adding a single edge $(n, 0)$ to the linear graph. We proceed by decomposing the true currents $i(x)$ [again taking the convention

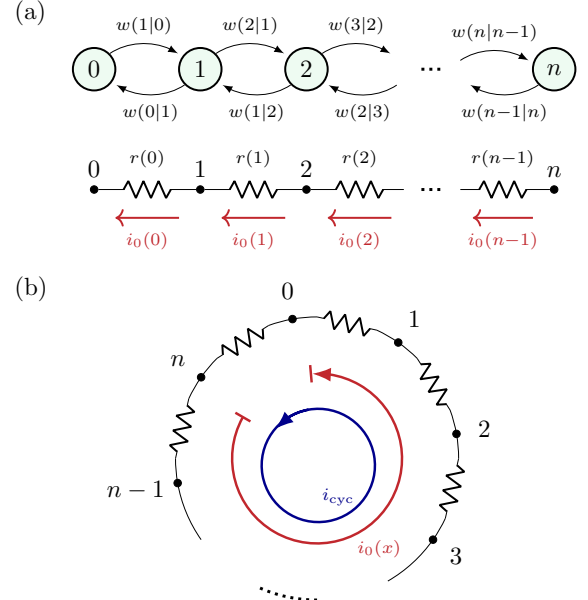


FIG. 1. (a) The Markov graph for a linear chain of states and its series circuit representation. The orientation of the edge currents i_0 reflect the convention in the main text. (b) Circuit representation of a cyclic Markov graph, with total currents $i(x)$ decomposed into a reference current $i_0(x)$ obtained by a cut along $(n, 0)$ and a cycle correction i_{cyc} .

that $i(x) = i(x, x + 1)$] into two parts:

$$i(x) = i_0(x) + i_{\text{cyc}}(x) . \quad (35)$$

Here, $i_0(x) = \dot{\Pi}(x)$ is a reference current that would flow under the same driving if the $(n, 0)$ edge were cut [so that $i_0(n) = 0$ in particular] and $i_{\text{cyc}}(x)$ is the cycle correction. Since $\dot{\pi}(x) = \sum_y i_0(x, y)$ by construction, then we must have

$$\sum_y i_{\text{cyc}}(x, y) = 0 \quad (36)$$

for all x . This is Kirchoff's current law without current injections – for a single cycle, this means that i_{cyc} is spatially uniform and in particular equal to the current $i(n)$ on the $(n, 0)$ edge.

The magnitude of i_{cyc} can be determined by Thompson's principle [7]: the currents $i(x)$ are those that uniquely minimize the power $\mathcal{P} = \sum_x r(x)[i(x)]^2$ subject to Kirchoff's current law, here Eq. (27). We obtain

$$\langle \mathcal{P}_{\text{ex}} \rangle^{(\text{LR})} = \mathcal{P}_0 - \frac{\mathcal{E}_{\text{cyc}}^2}{R_{\text{cyc}}} , \quad (37)$$

where $R_{\text{cyc}} \equiv \sum_{x=0}^n r(x)$ is the total resistance around the cycle, $\mathcal{E}_{\text{cyc}} \equiv \sum_{x=0}^n r(x)\dot{\Pi}(x)$ is the net “electromotive force” around the loop, and \mathcal{P}_0 is the dissipated power for the linear graph $\{0, \dots, n\}$ [Eq. (34)]. By expanding (37) in terms of an arbitrary control set as in

(34), we obtain

$$\tilde{\zeta}_{ij} = \tilde{\zeta}_{ij}^0 - \tilde{\zeta}_{ij}^{\text{cyc}} , \quad (38)$$

where $\tilde{\zeta}_{ij}^0$ is the friction for the linear graph and

$$\tilde{\zeta}_{ij}^{\text{cyc}} = \frac{\sum_{x,y} r(x) r(y) \partial_i \Pi(x) \partial_j \Pi(y)}{\sum_x r(x)} \quad (39)$$

is the reduction in the friction due to closure of the loop.

The strict negativity of the correction $-\mathcal{E}_{\text{cyc}}^2/R_{\text{cyc}}$ to the linear-chain excess power in Eq. (37) reflects Rayleigh's monotonicity theorem: adding an edge to the graph can never increase effective resistances [7]. Physically, the loop provides a parallel pathway that shunts probability flux. Moreover, for a distribution sufficiently localized away from the cut and slowly changing, the correction becomes negligible and the graph can effectively be treated as a linear graph. This follows from $R_{\text{cyc}} = \sum_x [w(x+1|x)\pi(x)]^{-1}$ and $\mathcal{E}_{\text{cyc}} = \sum_x \dot{\Pi}(x)/[w(x+1|x)\pi(x)]$: If we cut an edge $(x, x+1)$ where $\pi(x), \pi(x+1)$, and their time derivatives are all very small, then R_{cyc} will become very large while \mathcal{E}_{cyc} remains bounded.

This method is generalizable: Decompose the total currents into a reference current on the same nodes and apply Thompson's principle to find the correction currents (which in general will not be spatially uniform). This could be applied, e.g., to determine the sensitivity of the LR excess power to changes in the topology of the Markov graph.

VII. CONTINUOUS-STATE GENERALIZATION

The relationship between the LR dissipation and mean first-passage times established in Sec. III for finite reversible Markov chains extends (with minor modifications) to continuous-space processes.

First, observe that for discrete state spaces the MFPT from y to x can be expressed as the integral

$$\tau_{\text{mfp}}(x|y) = \frac{1}{\pi(x)} \int_0^\infty dt [p_t(x|x) - p_t(x|y)] , \quad (40)$$

with $p_t(x|y) = \exp\{t\mathbb{W}\}(x, y)$. This follows from (13) and the integral representation of the Drazin inverse of the rate matrix [19].

Consider now a reversible Markov process $(X_t)_{t \geq 0}$ on a continuous state space Ω with infinitesimal generator \mathcal{L}^\dagger , invariant density π , and transition kernel $p_t(x|y) = \exp\{t\mathcal{L}^\dagger\}(x, y)$ satisfying detailed balance $\pi(y)p_t(x|y) = \pi(x)p_t(y|x)$. For diffusion in a confining potential, Eq. (40) (with x, y now taken to be continuous variables) is precisely equal to the MFPT between points x and y for $\Omega = \mathbb{R}$ [33]. For higher dimensions, pointwise MFPTs diverge; however, under standard con-

ditions [17, 34] on \mathcal{L}^\dagger , the integrand in (40) goes to zero exponentially quickly, at a rate characterizing how fast the system erases its memory of originating at y with respect to the density at x . Thus, though Eq. (40) is no longer a true mean first-passage time for higher dimensions, it remains finite and characterizes a timescale of separation between x and y .

We define the *commute-time kernel* in terms of (40) as in Eq. (12). In B, we prove that the metric equivalence established in Sec. III holds for the continuous kernel: $\beta g \sim -\frac{1}{2}C$.

VIII. CONCLUSION

The geometry of slow driving in reversible Markov processes admits several representations, each offering different tools for interpretation and calculation. Through the graph Laplacian L , we have unified the friction metric with effective resistance, commute times, and discrete optimal transport restricted to paths of equilibrium distributions.

The electrical analogy offers powerful tools for calculation and interpretation. By treating the Markov graph as a resistor network, we derived exact friction metrics for linear and cyclic topologies. These results effectively demonstrate the more general observation that topological loops reduce LR thermodynamic cost via Rayleigh's monotonicity theorem. The mapping also leads to a direct probabilistic interpretation of LR dissipation. Simultaneously, the commute-time embedding provides intuition for the local geometry of the thermodynamic manifold and identifies bottlenecks as physical distances that require energy to traverse.

These results suggest several interesting directions for future research. For continuous harmonic potentials, exact minimizers of the excess work (beyond linear response) can be obtained from LR optimal protocols via a counterdiabatic correction [6]; though we have extended the LR control-OT correspondence here, it remains an open question whether analogous corrections can be constructed for discrete graph dynamics. Further work might explore non-reversible dynamics or control through nonconservative forces, leverage data-driven estimation of resistance metrics from simulation or experiment [35] for complex systems, or examine the implications of commute-time and bottleneck inequalities for efficient driving.

ACKNOWLEDGMENTS

We thank Antonio Patrón Castro and W. Callum Wareham (Simon Fraser University, Department of Physics) for feedback on the manuscript. This work was supported by NSERC CGS Master's and Doctoral scholarships (J.R.S.), an NSERC Discovery Grant RGPIN-2020-04950 (D.A.S.), and a Tier-II Canada Research

Appendix A: Connection of optimal transport formulation to previous work

We show here that the restricted L^2 -Wasserstein metric (22) defined in Section IV is a special case of the metric for probability transport on finite graphs developed in works such as [23, 24, 36]. Consider a weighted graph $G = (\Omega, \mathcal{E}, \omega)$ with vertex set Ω , edge set \mathcal{E} , and symmetric edge weights $\omega(x, y) = \omega(y, x) > 0$ for $(x, y) \in \mathcal{E}$. The discrete L^2 -Wasserstein distance between probability vectors p_0, p_1 on G is defined in [36] as

$$\mathcal{W}_2^2(p_0, p_1) \equiv \inf_{p_s = -\text{div}_G(p_s \nabla_G \phi_s)} \int_0^1 ds \|\nabla_G \phi_s\|_{p_s}^2. \quad (\text{A1})$$

The product $p \nabla_G \phi$ in the constraint is called a *flux function*, defined as

$$(p \nabla_G \phi)(x, y) \equiv \theta_p(x, y) \nabla_G \phi(x, y) \quad (\text{A2})$$

for some symmetric generalized mean $\theta_p(x, y)$ of $p(x)$ and $p(y)$, with divergence

$$\text{div}_G(p \nabla_G \phi)(x) = - \sum_y \sqrt{\omega(x, y)} \theta_p(x, y) (\nabla_G \phi)(x, y). \quad (\text{A3})$$

The gradient operator is $\sqrt{\omega}$ -weighted,

$$(\nabla_G \phi)(x, y) = \begin{cases} \sqrt{\omega(x, y)} [\phi(x) - \phi(y)] & (x, y) \in \mathcal{E}, \\ 0 & (x, y) \notin \mathcal{E} \end{cases}, \quad (\text{A4})$$

and the inner product with respect to p is

$$(v, w)_p \equiv \frac{1}{2} \sum_{(x, y) \in \mathcal{E}} v(x, y) \omega(x, y) \theta_p(x, y). \quad (\text{A5})$$

Under the restriction $p_s = \pi_s$, and ω, θ_p chosen such that

$$\omega(x, y) \theta_p(x, y) = w_\pi(x|y) \pi(y), \quad (\text{A6})$$

the L^2 -Wasserstein distance (A1) coincides exactly with the expression (22) for the thermodynamic distance. Here we have emphasized in the notation $w_\pi(x|y)$ that the rates depend on the equilibrium distribution.

The weights ω are π -independent and may refer to a fixed reference process. In the absence of physical motivation to the contrary, it is natural to take unit weights

$$\omega(x, y) = \begin{cases} 1, & (x, y) \in \mathcal{E} \\ 0, & (x, y) \notin \mathcal{E} \end{cases}, \quad (\text{A7})$$

so that

$$\theta_\pi(x, y) = w_\pi(x|y) \pi(y). \quad (\text{A8})$$

Under commonly chosen rate laws, $\theta_\pi(x, y)$ is indeed a generalized average. For instance, taking the rates $w_\pi(x|y) = \sqrt{\pi(x)/\pi(y)}$ that maximize trajectory entropy subject to detailed balance [37] gives

$$\theta_\pi(x, y) = \sqrt{\pi(x) \pi(y)}, \quad (\text{A9})$$

the geometric mean of the equilibrium probabilities. Glauber rates $w(x|y) = \pi(x)/[\pi(x) + \pi(y)]$ give

$$\theta_\pi(x, y) = \left[\frac{1}{\pi(x)} + \frac{1}{\pi(y)} \right]^{-1}, \quad (\text{A10})$$

the harmonic mean of the equilibrium probabilities. In [23, 24, 36], the generalized average $\theta_p(x, y)$ is chosen such that the dynamics are a gradient flow with respect to some entropy or free-energy functional. Though it is not clear whether such gradient-flow structures are relevant in this context, the forms of θ_p studied in [23, 24, 36] can be reproduced with suitable transition rates.

Appendix B: Commute-time kernel

We show here that a *commute-time kernel* $C(x, y)$ introduced in Section VII by analogy to the discrete commute-time matrix is metrically equivalent to the friction tensor for continuous systems. Let $p_t(x|y) = \exp\{t\mathcal{L}^\dagger\}(x, y)$ be the transition kernel of a continuous-space reversible Markov process with infinitesimal generator \mathcal{L}^\dagger . Define the *commute-time kernel*

$$C(x, y) \equiv \int_0^\infty dt \left[\frac{p_t(x|x) - p_t(x|y)}{\pi(x)} + \frac{p_t(y|y) - p_t(y|x)}{\pi(y)} \right]. \quad (\text{B1})$$

As discussed in Sec. VII, for $\Omega = \mathbb{R}$ this coincides with the actual commute time between points x and y . For $\Omega = \mathbb{R}^d$ with $d > 1$, the interpretation is less straightforward, though $C(x, y)$ still describes a timescale connecting points x and y .

Let \mathcal{A} and \mathcal{B} be real-valued functions on Ω (i.e., observables) such that $\langle \mathcal{A} \rangle_\pi = \langle \mathcal{B} \rangle_\pi = 0$. Then from the definition (B1),

$$\begin{aligned} \int_0^\infty dt \langle \mathcal{A}(X_t) \mathcal{B}(X_0) \rangle_{\text{eq}} \\ = -\frac{1}{2} \int_\Omega dx \int_\Omega dy \pi(x) \mathcal{A}(x) C(x, y) \mathcal{B}(y) \pi(y). \end{aligned} \quad (\text{B2})$$

(The $-1/2$ factor comes from the detailed-balance symmetry of the factors $-p_t(x|y)/\pi(x)$ and $-p_t(y|x)/\pi(y)$ in the integrand of $C(x, y)$.) Let $\mathcal{A}(X_t) = \hat{\omega}(x', X_t)$ and $\mathcal{B}(X_t) = \hat{\omega}(x'', X_t)$ be normalized indicator functions

$$\hat{\omega}(x, X_t) \equiv \frac{\delta(x - X_t) - \pi(x)}{\pi(x)} \quad (\text{B3})$$

at some fixed points $x', x'' \in \Omega$. Then

$$\int_0^\infty dt \langle \mathcal{A}(X_t) \mathcal{B}(X_0) \rangle_{\text{eq}} = \int_0^\infty dt \langle \hat{\omega}(x', X_t) \hat{\omega}(x'', X_t) \rangle_{\text{eq}} \quad (\text{B4a})$$

$$= \frac{1}{\pi(x') \pi(x'')} \int_0^\infty dt \langle [\delta(x' - X_t) - \pi(x')] [\delta(x'' - X_0) - \pi(x'')] \rangle \quad (\text{B4b})$$

$$= k_B T \frac{1}{\pi(x') \pi(x'')} \zeta(x', x'') \quad (\text{B4c})$$

$$= \beta g(x', x'') , \quad (\text{B4d})$$

where $\zeta(x', x'')$ is the integral kernel of the friction tensor on the global thermodynamic manifold [16], and the final

step follows from the change-of-variables formula

$$\zeta(x', x'') = \int dy' \int dy'' \frac{\delta\pi(y')}{\delta V(x')} \frac{\delta\pi(y'')}{\delta V(x'')} g(y', y'') . \quad (\text{B5})$$

Next, substituting $\mathcal{A}(X_t)$ and $\mathcal{B}(X_t)$ into the right-hand side of (B2) gives

$$-\frac{1}{2} \int_\Omega dx \int_\Omega dy \pi(x) \mathcal{A}(x) C(x, y) \mathcal{B}(y) \pi(y) = -\frac{1}{2} \int_\Omega dx \int_\Omega dy C(x, y) [\delta(x - x') - \pi(x')] [\delta(y - x'') - \pi(x'')] \quad (\text{B6a})$$

$$= -\frac{1}{2} C(x', x'') + k_1 \pi(x') + k_2 \pi(x'') , \quad (\text{B6b})$$

for constants k_1, k_2 . Since $\int_\Omega dx \dot{\pi}(x) = 0$, these constant-coefficient terms vanish in the LR excess power

$$\langle \mathcal{P}_{\text{ex}} \rangle^{(\text{LR})} = \int_\Omega dx \int_\Omega dy g(x, y) \dot{\pi}(x) \dot{\pi}(y) , \quad (\text{B7})$$

and thus $\beta g \stackrel{\Delta^n}{\sim} -\frac{1}{2} C$.

[1] F. Weinhold, Metric geometry of equilibrium thermodynamics, *J. Chem. Phys.* **63**, 2479 (1975).

[2] P. Salamon and R. S. Berry, Thermodynamic length and dissipated availability, *Phys. Rev. Lett.* **51**, 1127 (1983).

[3] G. Ruppeiner, Riemannian geometry in thermodynamic fluctuation theory, *Rev. Mod. Phys.* **67**, 605 (1995).

[4] S. Ito, Stochastic thermodynamic interpretation of information geometry, *Phys. Rev. Lett.* **121**, 030605 (2018).

[5] D. A. Sivak and G. E. Crooks, Thermodynamic metrics and optimal paths, *Phys. Rev. Lett.* **108**, 190602 (2012).

[6] A. Zhong and M. DeWeese, Beyond linear response: Equivalence between thermodynamic geometry and optimal transport, *Phys. Rev. Lett.* **133**, 057102 (2024).

[7] P. G. Doyle and J. L. Snell, Random walks and electric networks (2000), arXiv:math/0001057 [math.PR].

[8] A. Ghosh, S. Boyd, and A. Saberi, Minimizing effective resistance of a graph, *SIAM Rev.* 10.1137/050645452 (2008).

[9] D. A. Spielman and N. Srivastava, Graph sparsification by effective resistances, *SIAM J. Comput.* **40**, 1913 (2011).

[10] Y. Deng, Q. Dai, R. Wang, and Z. Zhang, Commute time guided transformation for feature extraction, *Comput. Vis. Image Underst.* **116**, 473 (2012).

[11] K. Fitch, Effective resistance preserving directed graph symmetrization, *SIAM J. Matrix Anal. Appl.* **40**, 49 (2019).

[12] J. R. Sato, C. M. Sato, M. K. d. C. Silva, and C. E. Biázoli, Commute time as a method to explore brain functional connectomes, *Brain Connect.* **9**, 155 (2019).

[13] P. G. Doyle and J. Steiner, Commuting time geometry of ergodic Markov chains (2017), arXiv:1107.2612 [math].

[14] A. K. Chandra, P. Raghavan, W. L. Ruzzo, and R. Smolensky, The electrical resistance of a graph captures its commute and cover times, in *Proceedings of the twenty-first annual ACM symposium on Theory of computing - STOC '89* (ACM Press, Seattle, Washington, United States, 1989) pp. 574–586.

[15] D. J. Klein and M. Randić, Resistance distance, *J. Math. Chem.* **12**, 81 (1993).

[16] J. R. Sawchuk and D. A. Sivak, Global thermodynamic manifold for conservative control of stochastic systems (2025), arXiv:2409.18065 [cond-mat].

[17] G. Wang, Y. Wei, and S. Qiao, *Generalized Inverses: Theory and Computations*, Developments in Mathematics, Vol. 53 (Springer, Singapore, 2018).

- [18] M. Yadav and K. Thulasiraman, Network science meets circuit theory: Kirchhoff index of a graph and the power of node-to-datum resistance matrix, in *ISCAS*, Vol. 2015-(IEEE, New York, 2015) pp. 854–857.
- [19] P. Coolen-Schrijner and E. A. van Doorn, The deviation matrix of a continuous-time Markov chain, *Probab. Eng. Inf. Sci.* **16**, 351 (2002).
- [20] J.-D. Benamou and Y. Brenier, A computational fluid mechanics solution to the Monge–Kantorovich mass transfer problem, *Numer. Math.* **84**, 375 (2000).
- [21] F. Otto, The geometry of dissipative evolution equations: The porous medium equation, *Commun. Partial Differ. Equ.* **26**, 101 (2001).
- [22] L. J. Grady and J. R. Polimeni, *Discrete Calculus: Applied Analysis on Graphs for Computational Science* (Springer-Verlag London, 2010).
- [23] J. Maas, Gradient flows of the entropy for finite Markov chains, *J. Funct. Anal.* **261**, 2250 (2011).
- [24] S.-N. Chow, W. Huang, Y. Li, and H. Zhou, Fokker–Planck equations for a free energy functional or Markov process on a graph, *Arch. Ration. Mech. Anal.* **203**, 969 (2012).
- [25] J. Wang, Classical Multidimensional Scaling, in *Geometric Structure of High-Dimensional Data and Dimensionality Reduction*, edited by J. Wang (Springer Berlin Heidelberg, Berlin, Heidelberg, 2012) pp. 115–129.
- [26] R. Zwanzig, Dynamical disorder: Passage through a fluctuating bottleneck, *J. Chem. Phys.* **97**, 3587 (1992).
- [27] D. Chakrabarti and B. Bagchi, Waiting time distribution and nonexponential relaxation in single molecule spectroscopic studies: Realization of entropic bottleneck in a simple model, *J. Chem. Phys.* **118**, 7965 (2003).
- [28] D. Mandal and C. Jarzynski, Analysis of slow transitions between nonequilibrium steady states, *J. Stat. Mech.: Theory Exp.* **2016** (6), 063204.
- [29] J. E. Avron, M. Fraas, G. M. Graf, and P. Grech, Adiabatic theorems for generators of contracting evolutions, *Commun. Math. Phys.* **314**, 163 (2012).
- [30] F. Dorfler and F. Bullo, Kron reduction of graphs with applications to electrical networks, *IEEE Trans. Circuits Syst. I: Regul. Pap.* **60**, 150 (2013).
- [31] P. R. Zulkowski and M. R. DeWeese, Optimal control of overdamped systems, *Phys. Rev. E* **92**, 032117 (2015).
- [32] T. Van Vu and K. Saito, Thermodynamic unification of optimal transport: Thermodynamic uncertainty relation, minimum dissipation, and thermodynamic speed limits, *Phys. Rev. X* **13**, 011013 (2023).
- [33] D. J. Bicout and A. Szabo, First passage times, correlation functions, and reaction rates, *J. Chem. Phys.* **106**, 10292 (1997).
- [34] G. A. Pavliotis, *Stochastic Processes and Applications: Diffusion Processes, the Fokker-Planck and Langevin Equations*, Vol. 60 (Springer Nature, New York, 2014).
- [35] F. Noé, R. Banisch, and C. Clementi, Commute maps: Separating slowly mixing molecular configurations for kinetic modeling, *J. Chem. Theory Comput.* **12**, 5620 (2016).
- [36] S.-N. Chow, W. Li, and H. Zhou, Entropy dissipation of Fokker–Planck equations on graphs, *Discrete Contin. Dyn. Syst.* **38**, 4929 (2018).
- [37] P. D. Dixit, A. Jain, G. Stock, and K. A. Dill, Inferring transition rates of networks from populations in continuous-time Markov processes, *J. Chem. Theory Comput.* **11**, 5464 (2015).